CHAPTER 8: CONVERSION OF NON-DUCTILE CHEVRON BRACE INTO STIFFENED-CASING DUAL-SLEEVE BUCKLING RESTRAINED BRACE

The eccentric NCBFs were upgraded to a very good degree but little strength degradation (*less ductile*) was observed in the hysteresis curves of the chevron braced frames even after the modifications. A method to improve the inelastic behavior of the non-ductile concentric braced frames (NCBFs) under cyclic/ repeated loading has been presented in this section. As a reference NCBF specimen, an old (*pre-1970*) experimentally tested steel braced frame having concentric chevron braces was analyzed in the FEM based simulation software, using shell elements.

The analysis included both geometric and material non-linearities. After the buckling of a brace, chevron NCBFs experienced serious strength degradation, excessive beam deflection, the condition of ineffective tension-brace and at higher loading it experienced excessive levels of stresses. Here, a strategy was devised for the renovation of NCBFs which would avoid the detrimental effects of the bucking of the braces. It would provide excellent inelastic behavior to the existing NCBFs making them ductile and effective against the seismic loading. For this purpose, chevron brace in the old NCBF were converted to a stiffened-casing dual-sleeve buckling restraint brace (SCDS-BRB), without replacing any member of the steel braced frame.

8.1 METHODOLOGY

To devise the method for the upgrade an older steel braced frames (NCBFs), all the necessary specifications (*both geometrical and material*) of such older specimen for modelling and analyzing were required. For this purpose, experimentally tested (pre-1970) concentric chevron braced steel frames (Wakabayashi and Tsuji 1967) were

chosen. The specimens were modelled on the Abaqus CAE platform (2017). All the members were modelled using 4-node doubly curved thin shell (S4R) element (*with hourglass control*), as shown in Figure 8.1. Both geometric and material non-linearities were included in the analysis. Tri-linear stress-strain curve was implemented along with the half-cycle combined hardening effect.

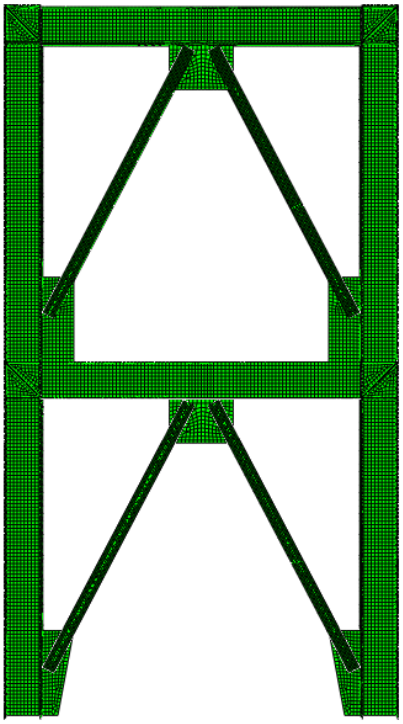

i) Meshed two-story specimen

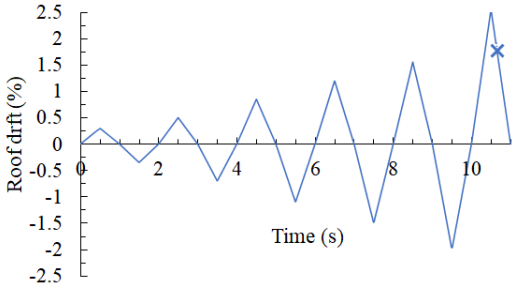

ii) Single-story braced frame loading

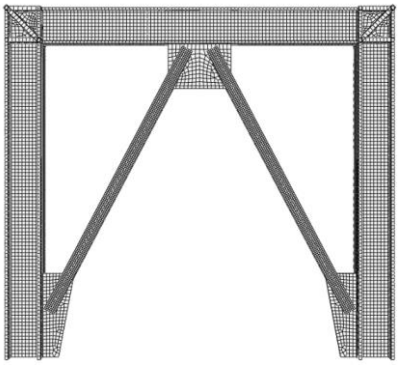

iii) Meshed single-story specimen

Figure 8.1 Meshing of the chevron braced frames and the displacement loading on them

In the analysis, density, young's modulus, Poisson's ratio and damping factor were 7,850 kg/m^3, 2.1×10^5 MPa, 0.3 and 0.02 respectively. The material properties obtained in the coupon test results (*adapted from the experimental results reported by Wakabayashi and Tsuji 1967*) for each member made-up of JIS-SS41 steel have been given in the Table 8.1. The actual section dimensions were utilized for the purpose of analysis. The displacement loading was given in an incremental manner (*roof drift %*), as shown in Figure 8.1 (ii).

Table 8.1 Member sections and their material properties

Member	Standard Section (mm)	Actual Section (mm)	σ_y (MPa)	σ_u (MPa)	ϵ_p
Column	H-100×100×6×8	H-101×100×6×8	255	412	0.27
Beam	H-100×50×5×7	H-101×49.5×4.2×6.3	306	435	0.20
Braces	H-40×30×4×4	H-40.5×32×4.6×4.6	278	429	0.24

Note: σ_y is the yield stress, σ_u is the ultimate stress and ϵ_p is the plastic strain.

The analysis results of the two-story specimen matched with the experimental results to a very good extent. In the experimental report, the member specifications were same for both two-story and single-story chevron braced frames. As the analysis of the converted BRBs required a continuous and extensive use of contact-based interaction, the single-story specimen (*Ch_S1*) was selected for the further modifications.

As per the given geometrical specifications of the older experimented NCBF specimen, in-plane buckling of the braces was expected. According to AISC (2016) seismic provision, the local slenderness criteria (*refer Equations 7.1 to 7.4*) for members in a braced frame has been defined by flange-width to flange-thickness ratio (b/t_f) and web-height to web-thickness ratio (h/t_w). Unlike the NCBFs numerically tested by Narayan and Pathak (2021, 2022); here, some members of the experimented specimen didn't satisfy both the local and global slenderness criteria even after considering R_y value equal to 1 (R_y *= 1.5 was used by Narayan and Pathak (2021, 2022), which was the highest value as per AISC 2016*) for JIS-SS41 steel (*equivalent to the ASTM-A36 steel*).

The column lacked in b/t ratio (*even with* $R_y = 1$), as its value was 12.5, instead of being less than the design value of 11.5 (*still, the columns behaved properly in all cases*). The global slenderness ratio of the braced frame was 124 (*the effective length was calculated using the methodology described by Narayan et. al. 2020*), instead of being less than the design value of 110 (*maximum allowable slenderness ratio for a brace as per AISC 2016, IS:800 2007 and JSCE 2009 can be 200, 120 and 120 respectively*).

As a parameter for studying the structural behaviour of the chevron braced frames, strength ratio '*C*' (*refer Equation 7.5*) was used by Tsuji and Nishino (1988). There, the beams were found to deflect elastically for the braced frame having high '*C*' value (1.1). Large vertical displacement of beams took place for the braced frames having small '*C*' value (0.5, 0.8). In the study presented here, '*C*' value of the selected NCBF specimen was 0.85, considering L_b as overall length of the brace. Irrespective of the strong-beam suggestion by AISC (2016), as per Sen *et. al*. (2014, 2019), chevron NCBFs having weak-beams (*but with SCBF compliant braces*) had seismic response similar to well-designed SCBFs. In the numerical analysis of an older NCBF by Narayan and Pathak (2022), even-though all the members of the frames satisfied the SCBF criteria, but still significant strength degradation was observed. So, there, the '*C*' value equal to '0.7' was found to be more compatible with the observed results. Here also, in the present study, the beam was found to satisfy the all the local and global slenderness criteria (*according to AISC (2016) such beam was expected to provide a SCBF like structural behaviour to the braced frame, but it wasn't found to do so*). Here in present specimen, weak-beam behaviour was portrayed by beams as expected for braced frame with '*C*' value of 0.85.

Each story height was 1 m and all the joints were welded (*modelled using rigid tie connection*). Beam-column end connections were restrained in out-plane direction and the base supports were fixed. For connecting the braces to the frame, 6 mm thick gusset plates were used. To avoid yielding of the frame panel, 12 mm thick diagonal stiffener plates were fitted at the beam-column connection ends. Here, the maximum story drift was 2.5% (*AISC (2016) recommends at-least 2% drift for testing buckling restrained braced frames, BRBFs*) and the drift range was 4.5%. The purpose was to obtain a buckling restrained brace (BRB) arrangement which could provide a stable and balanced hysteretic behavior, at-least above the drift range causing failure of the selected NCBF.

Table 8.2 Description of various arrangements of the generated BRBs

Symbol	Deformation of core	Remark
Ip	Expected in-plane	gap in-plane; restrained out-plane
IpW	Expected in-plane	20 cm long/ 20 mm wide transition ends of core
Int	Expected out-plane	gap provided out-plane; restrained in-plane (using internal filler plate)

Referring Table 8.1, the available space in the braces for the modifications included the clear depth of its web portion (*31.3 mm, transverse direction*) and the width of the flange (*32 mm, lateral direction*). It was utilized in such a way that it would result in an effective configuration of the stiffened-casing dual-sleeve brace (SCDS-BRB). The description and the specifications of the finalized cases have been given in Table. 8.2 and 8.3 respectively. Out of many trails for developing a BRB from an existing brace, the obtained configurations were such that there was one primary sleeve (*called casing*) to restrain the generated buckling modes of the core and a secondary sleeve to prevent the wide opening of grooved mouth of casing, so as to limit the rotation of the brace just outside the core.

Table 8.3 Specifications of BRB specimens axial load analysis results

Type	l_c (mm)	b (mm)		G_l (mm)	G_{tr} (mm)	t_c (mm)	B	ω	$B\omega$
Ip	300 +20	15		0.15	2.70	4.6	1.11	1.27	1.41
IpW	300 – 20	15		0.15	2.70	4.6	1.5	1.02	1.53
Int	300 + 20	15		0.60	0.20	4.6	1.20	1.06	1.27

Note: l_c, b and t_c represent yielding length, width and thickness of core respectively; G_l, G_{tr} represents lateral and transverse gap inside casing for the plastic deformation of core respectively. 'β' and 'ω' are compression strength adjustment factor and strain hardening adjustment factor respectively (*derived from the hysteresis curves*).

For better comparison, the core/ casing/ secondary sleeve had thickness same as that of the existing brace (4.6 mm) and the core part in all of them had same width (15 mm) and over-all length of 300 mm (*+20 mm for groove*). As shown in Figure 8.2, the length of the flange removed from the middle portion of the clear length (0.61 m) of the existing brace was 0.3 m (*close to half of the clear length of the brace*) and the 20 cm long grooves were provided in the web of the brace to hold the casing at the bottom, around the core.

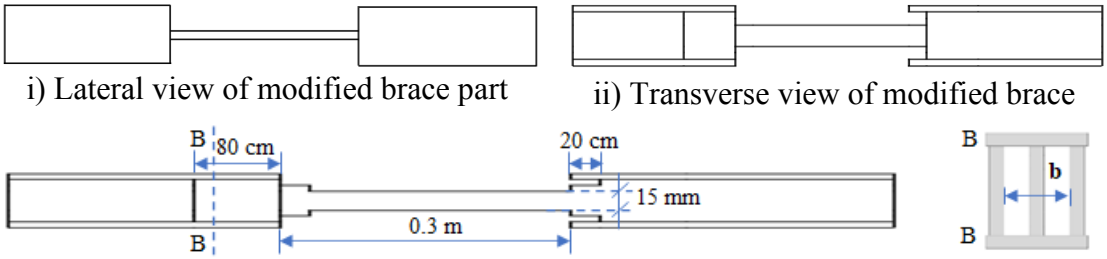

Figure 8.2 Details of the modified state of the existing brace (not to scale)

The length of the open box shaped secondary sleeves (shown in Figure 8.2 (iv)) around the web was 0.08 m (*outside the buckling mechanism portion; i.e.,next to the top end of the core*). As shown in Figure 8.3 (i), the length of the casing was 0.38 m and the length of the groove cut in casing at the top for its movement relative to the core, was 0.1 m.

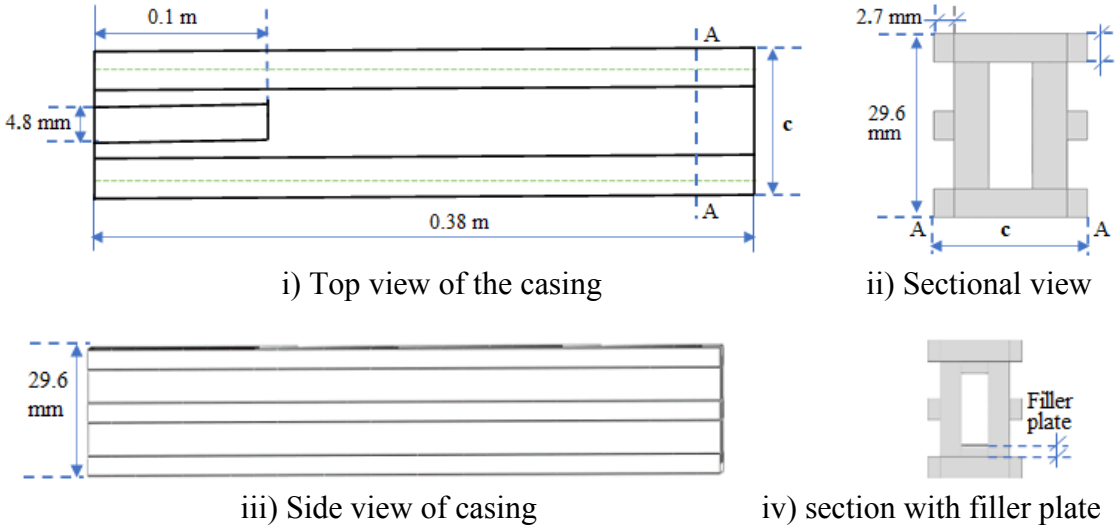

Figure 8.3 Details of geometry and cross-sections of casing (not to scale)

The total gap between casing and the inner surfaces of the flanges and the total gap between casing and secondary sleeve were 1.7 mm and 0.5 mm (*equal to 'b - c', according to Figure 8.2 and 8.3*) respectively. Because casing is the buckling restraining component of the BRB, it has always been recommended to use casing of higher stiffness. Casing was stiffened using 2.7 mm thick and 4.6 mm wide stiffener strips throughout its length (*on both the sides at upper end, lower end and at middle*), as shown in Figure 8.3.

8.2 RESULTS AND DISCUSSION

Single-story specimen experienced very high stresses for the given cyclic loadings. As observed in experimental report, it failed prematurely even at low number of loading cycles without giving a proper hysteresis curve. So, the loading used to validate the results of analysis of the corresponding two-story specimen was used here (*in terms of drift (%), Figure 8.1 (ii)*) to achieve proper hysteresis curves for better comparison of results.

The maximum stress in the single-story chevron braced specimen (*indicated by arrow in Figure 8.4 (i)*) was 408 MPa. It was observed at the bottom of the beam-column connection (*on the compression brace side*). Such high stress was completely localized in the beam leaving the column experiencing significantly low stresses. The stress in beam was very close to ultimate strength of its flange plate.

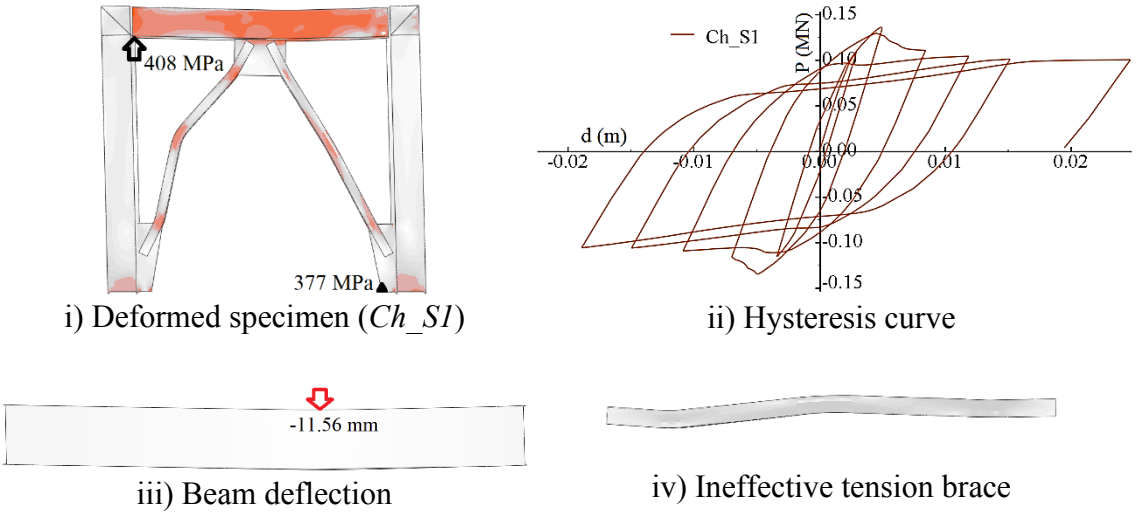

i) Deformed specimen (*Ch_S1*)

ii) Hysteresis curve

iii) Beam deflection

iv) Ineffective tension brace

Figure 8.4 Analyzed single-story concentric chevron braced frame (*Ch_S1*)

Here, the maximum stress in the brace-column connection (*377 MPa, indicated by triangular dot in Figure 8.4 (i)*) was observed at the support on the side opposite to the compression brace. It can be deducted from the hysteresis curve (shown in Figure 8.4 (ii)) that the serious strength degradation of the lateral load bearing capacity of the specimen

was observed after the initial buckling of braces (*initial peaks*). As shown in Figure 8.4 (iii) and (iv), the tension brace became ineffective (*remained in compression*) after the excessive downward deflection of the beam.

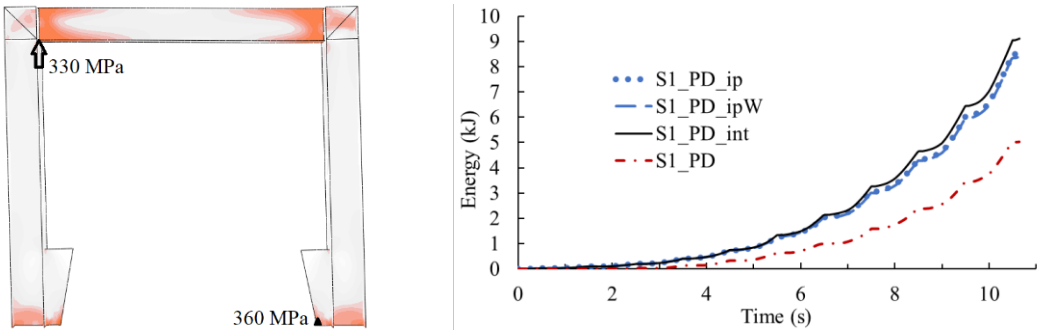

i) Bare Frame stresses ii) Plastic (energy) dissipation (*PD*)

Figure 8.5 Stresses in bare frame and comparison of energy dissipation (*PD*)

As shown in Figure 8.5 (i), unlike the braced frame specimens, the bare moment frame experienced the maximum stress at the bottom support (360 MPa), which was more than the stress experienced by it at the beam-column connection (330 MPa). Generally, the bare frames have been found to be more ductile but weaker as they would require very heavy sections to dissipate sufficient amount of energy generated during the occurrence of even a moderate earthquake.

It can also be seen in the Figure 8.5 (ii) that all the BRBF specimens (*with ip, ipW, int type BRBs*) could safely dissipate significantly higher energy than the bare frame. The energy dissipated by the BRBF having same width of the BRB core throughout undergoing in-plane deformation of its core (*S1_PD_ip; i.e., 8.57 kJ*) was little higher than the specimen having transition ends (*wider ends*) of the core (*S1_PD_ipW; i.e., 8.40 kJ*). The energy dissipated by the specimen having out-plane deformation of casing (*S1_PD_int; i.e., 9.11 kJ*) was close to twice of the energy dissipated by the bare frame (*S1_PD; i.e., 5.03 kJ*).

8.2.1 BRBF having in-plane deformation of core of BRB (*S1_BRB_ip*)

This type of BRB was formed by combining the specifications given in Figure 8.2 (*i, ii, iv*) and Figure 8.3 (*i, ii, iii*), i.e., the core section was 15 mm wide through-out its length and the thickness of the core was 4.6 mm (*as the web section of unmodified brace was 4.6 mm thick*). Referring '*ip*' type BRB in Table 8.3, the gap between the surface of the core and the inner walls of the casing in transverse direction of the core was 2.7 mm. For the comparison purpose, the height of casing was kept constant for all the selected specimens. So, the gap was a bit high but the critical buckling load of core was also higher in this direction. Core was restrained in the lateral direction with a gap of 0.15 mm to avoiding skidding and friction (*otherwise, small spikes at the time of unloading from the tensile load would have been prominent in the hysteresis curves*).

i) Stress in '*ip*' type BRBF ii) Deformation of BRB (*ip*) core

Figure 8.6 Stresses in BRBF (*S1_BRB_ip*) and deformation of its BRB core

It can be clearly observed in the Figure 8.6 (i) that the induced stresses were significantly lower than for the bare frame specimen and extremely lower than the braced specimens (NCBFs). Unlike the bare frame and NCBF specimens, the connection zones were not the most stressed zones here. The maximum stress was observed at the southern base-support (330 MPa). As shown in Figure 8.6 (ii), three-node deformation was observed in the core of the BRB, which was good enough for the in-plane deformation of core. The

maximum stress in the beam was found at the southern side near the top of the beam-column connection (*320 MPa, shown by arrow*). Maximum stress in the beam observed for the single-story specimen was 371 MPa, which was next to the overall maximum stress (i.e., *at the beam-column joint, 408 MPa, shown by arrow in Figure 8.4*).

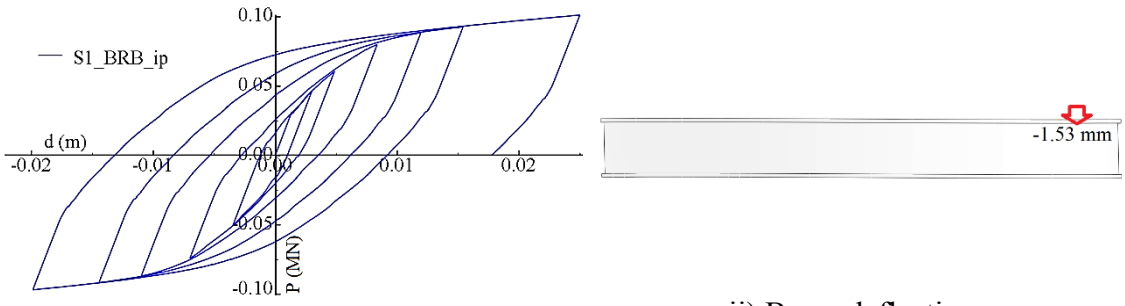

i) Hysteresis curve ii) Beam deflection

Figure 8.7 Hysteresis curve of BRBF (*S1_BRB_ip*) and deflection of its beam

No strength degradation was observed in the hysteresis curve. Hysteresis curve was both stable and symmetric (shown in Figure 8.7 (i)). As per AISC (2016), the BRB parameters 'β' and '$\beta\omega$' should be more than 1 and less than 1.5, whereas the 'ω' value should be greater than 1. Referring Table 8.3 for the '*ip*' type BRB, these parameters were found to be within the permissible limits for this BRB-type specimen.

Here, the downward beam deflection (shown in Figure 8.7 (ii)) was just 1.53 mm, whereas it was 11.56 mm in the case of single-story chevron braced frame specimen (*there, the tension brace become ineffective*).

8.2.2 BRBF having in-plane deformation of core (*having wide-ends*) of BRB (*S1_BRB_ipW*)

This type of BRB was formed by combining the specifications given in Figure 8.2 (*i, iii, iv*) and Figure 8.3 (*i, ii, iii*), i.e., the core section was 15 mm wide and had transition ends (*20 mm wide core for 20 cm length*) and the thickness of the core was 4.6 mm. Referring

to the '*ipW*' type BRB in Table 8.3, the gap between the surface of the core and the inner walls of the casing in transverse direction of the core was 2.7 mm. Core was restrained in the lateral direction with a gap of 0.15 mm to limit unwanted skidding and friction.

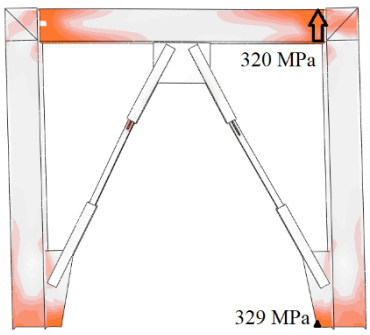

i) Stress in '*ipW*' type BRBF

ii) Deformation of BRB (*ipW*) core

Figure 8.8 Stresses in BRBF (*S1_BRB_ipW*) and deformation of its BRB core

It can be clearly observed in the Figure 8.8 (i) that the maximum stress was observed at the southern base-support (329 MPa). As shown in Figure 8.8 (ii), three-node deformation was observed in the core of the BRB, which was good enough for the in-plane deformation of core. The maximum stress in the beam was found at the southern side near the top of the beam-column connection (*320 MPa, shown by arrow*).

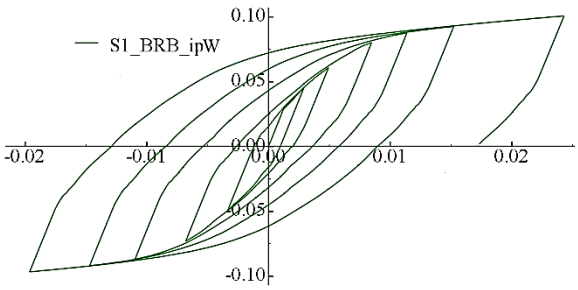

i) Hysteresis curve

ii) Beam deflection

Figure 8.9 Hysteresis curve of BRBF (*S1_BRB_ipW*) and deflection of beam

No strength degradation was observed in the hysteresis curve. Hysteresis curve was both stable and symmetric (shown in Figure 8.9 (i)). Here, the downward beam deflection (shown in Figure 8.9 (ii)) was just 1.60 mm, whereas it was 11.56 mm in the case of

single-story chevron braced frame specimen. As per AISC (2016), the BRB parameters 'β' and '$\beta\omega$' should be more than 1 and less than 1.5, whereas the 'ω' value should be greater than 1. Referring Table 8.3 for the '*ipW*' type BRB, the permissible limits of the parameters weren't satisfied by this BRB-type specimen, as the 'β' value was equal to 1.5 and '$\beta\omega$' value was higher than 1.5.

8.2.3 BRBF having out-plane deformation of core of BRB (*S1_BRB_int*)

This type of BRB was formed by combining the specifications given in Figure 8.2 (*i, ii, iv*) and Figure 8.3 (*i, iii, iv*), i.e., the core section was 15 mm wide through-out its length and the thickness of the core was 4.6 mm. Referring '*int*' type BRB in Table 8.3, the gap between the surface of the core and the inner walls of the casing in lateral direction of the core was 0.6 mm. Core was restrained in the transverse direction with a gap of 0.2 mm.

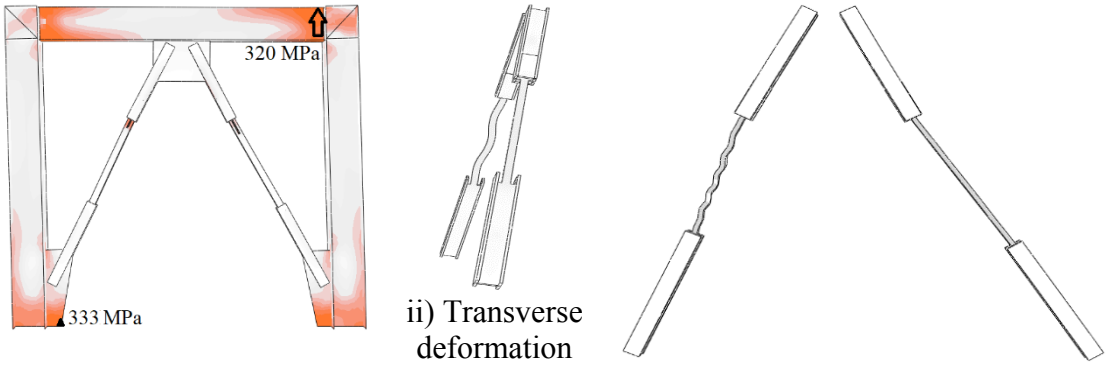

i) Stress in '*int*' type BRBF ii) Transverse deformation of core iii) Lateral deformation of core

Figure 8.10 Stresses in BRBF (*S1_BRB_int*) and deformation of its BRB core

Unlike the other two BRB types, the maximum stress was observed at the northern bottom support (333 MPa), as shown in Figure 8.10 (i). Even-though the space provided between the core and the walls of the casing in the transverse direction was very small but the space between the depth of the casing and the clear depth of the web of the original brace was 1.7 mm, which made it to dissipate the energy through transverse deformation also (as shown in Figure 8.10 (ii)). In many of the all-steel BRBs developed previously, this

state of transverse deformation along with the lateral deformation can be observed. As shown in Figure 8.10 (iii), a yielding deformation in the form of quite a symmetrical nodal displacement was obtained (*the rotational deformation was minute so, it was scaled-up three times for better visibility*). The maximum stress in the beam was found at the southern side near the top of the beam-column connection (*320 MPa, shown by arrow*), which was equal in all the three selected BRBF specimens.

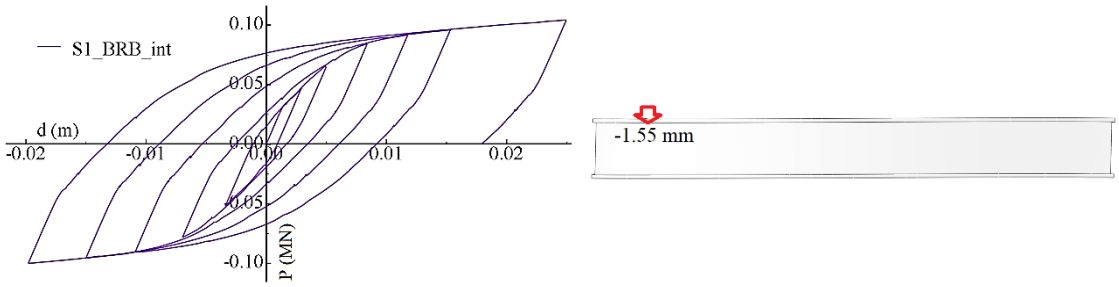

i) Hysteresis curve ii) Beam deflection

Figure 8.11 Hysteresis curve of BRBF (*S1_BRB_int*) and deflection of beam

No strength degradation was observed in the hysteresis curves. Hysteresis curve was both stable and symmetric (shown in Figure 8.11 (i)). Referring Table. 8.3 for the '*int*' type BRB, the design parameters were found to be within the permissible limits for this BRB-type specimen. Here, the downward beam deflection (shown in Figure 8.11 (ii)) was just 1.55 mm, whereas it was 11.56 mm in the case of single-story chevron NCBF specimen.

This BRBF having '*int*' type BRB worked better than other selected BRBFs, as the plastic dissipation of this BRBF was significantly higher than those BRBFs (*ip, ipw*). Unlike many other previously developed BRB types, the lateral deformation of the core was quite symmetrical and the casing didn't buckle locally/ globally and no local bulging was observed in the casing of any of the successful specimens (*ip, ipW, int*).

8.3 SOME OTHER IMPORTANT CONSIDERATIONS

While developing the buckling restraining mechanism, the use of smaller cores caused excessive rotation of the upper end of the core, which made the axial load transfer from core to casing, quite ineffective. Longer cores resulted in lower strength and limited the length of the secondary sleeve. Mirtaheri, Sehat. and Nazeryan (2018) suggested to improve the behavior of buckling restrained braces through obtaining optimum steel core length. So, the core length of about half of the clear length of the brace was chosen and it was found to work well in the selected specifications of the specimens.

One unsuccessful attempt to get a BRB configuration from the existing configuration of the chevron brace has also been shown in Figure 8.12 (i). There, the absence of the insertion of the casing inside the secondary sleeves (*absence of secondary sleeves*), caused the brace to fail pre-maturely with almost no benefit against lateral loading. So, the BRB brace configuration would not have been achieved in such case because of the excessive deformation/ rotation next to the core part. According to AISC (2016), the rotational demand can be concentrated in the region just outside the buckling restraining mechanism. the BRB must be tested for axial and rotational deformations.

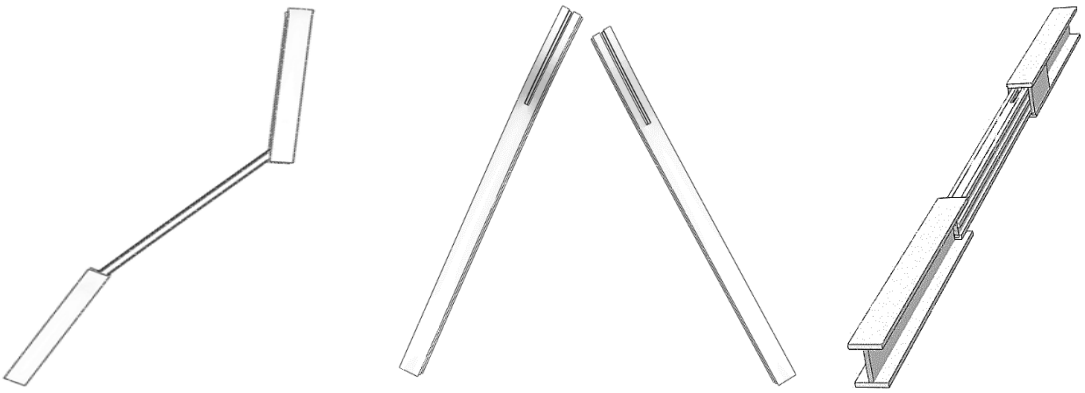

i) Excess rotation (failed trail) ii) Casing rotation (succesful trails) iii) Full BRB

Figure 8.12 Rotation of the brace just outside the buckling restraining mechanism

This requirement of AISC (2016) was justified; as the major cause of the failed trails was the rotation at the ends of the core. In all the three successfully working cases, the expected rotation of the ends of the core was minimal and the stiffened casing experienced minute rotation at its section just outside the buckling restraining mechanism (*shown in Figure 8.12 (ii), higher stress with darker shades*). Rotation here was not detrimental as the rotation was restrained by the secondary sleeve in these cases. Even-though the unstiffened casing 'with' secondary sleeve also worked satisfactorily in some trail cases but the energy dissipation was low in comparison to the BRBF specimens having stiffened casing. Full BRB specimen showing casing inserted in the secondary sleeve (t*op*) and held at bottom in the grooves has been shown in Figure 8.12 (iii).

8.4 CONCLUDING REMARKS

To improve the hysteretic behaviour of the CBFs, the existing chevron braces were converted into a new type of buckling retrained brace, which was called here as the stiffened-casing dual-sleeve BRB (SCDS-BRB). The problem of the excessive stress concertation, high initial peaks observed in the hysteresis curves resulting from buckling of braces and strength degradation at the later stages of loading, all were rectified using the developed SCDS-BRB configuration. Conclusions have been discussed elaborately in the last chapter, 'SUMMARY AND CONCLUSIONS'.